Full Length Article

g-C$_6$N$_6$ monolayer: A highly sensitive molecule sensor for biomarker volatiles of liver cirrhosis

W.X. Zhang [a], H.M. Yan [a], C. He [b],[*]

[a] School of Materials Science and Engineering, Chang'an University, Xi'an 710064, China
[b] State Key Laboratory for Mechanical Behavior of Materials, School of Materials Science and Engineering, Xi'an Jiaotong University, Xi'an 710049, China

ARTICLE INFO

ABSTRACT

Liver cirrhosis is often detected by complex method such as liver biopsy. At present, the best way to achieve rapid detection is to detect the biomarkers volatiles of liver cirrhosis from the breath of human, such as CH$_4$O, 2-pentanone and limonene. Herein, the structure, electronic structure and adsorption behavior of three liver cirrhosis biomarkers on g-C$_6$N$_6$ are investigated by using density functional theory. The results show that g-C$_6$N$_6$ monolayer has suitable adsorption energies for CH$_4$O (0.55 eV), 2-pentanone (0.68 eV) and limonene (0.81 eV), respectively. The adsorption and desorption behaviors of biomarker volatiles can be easily regulated through the strain and electric field, so as to realize the reversible detection of liver cirrhosis. Moreover, the optical properties before and after adsorption of CH$_4$O, 2-pentanone and limonene also changes obviously compared with the primitive g-C$_6$N$_6$ monolayer, indicating that the possibility of g-C$_6$N$_6$ monolayer as an optical gas sensor. The adsorption peak moves from blue light to purple light region, and the intensity of the peak also increases. This report paves the way for the possible application of g-C$_6$N$_6$, which shows a good response to the biomarker volatiles of liver cirrhosis.

1. Introduction

Cirrhosis is a kind of diffuse liver damage caused by one or more reasons. It can make a large number of stem cells necrosis, leading to gradual deformation, fibrosis and hardening of the liver. Cirrhosis can be detected by routine-blood test, liver function test, ascites examination, liver biopsy and other methods [1]. However, the early symptoms of liver cirrhosis are not obvious, and few people have targeted complex detection of liver cirrhosis. At present, there is no cure for cirrhosis. Most patients with advanced liver cirrhosis live less than 5 years. Liver transplantation and splenectomy can only be used to alleviate and temporarily improve the condition in the late stage of liver cirrhosis. The operation is complex and expensive, so it is very important to find the condition in the early stage of liver cirrhosis and treat it in time [2]. More simple and faster methods are needed to detect liver cirrhosis. Biomarkers are biochemical indicators that can mark the changes or possible changes in the structure or function of systems, organs, tissues, cells and sub cells. They are abnormal signal indicators at different biological levels (molecules, cells, individuals, etc.) due to the impact of environmental pollutants. Before the organisms are seriously damaged,

they can provide early warning for serious toxic injury [3]. According to previous reports, biomarkers can be used to detect diseases. For example, Davis et al. have investigated the relationship between biomarkers in exhaled breath condensate and the severity of pneumonia and sepsis [4]. Combined with biomarkers, prostate specific antigen (PSA), microRNAs and adenogen receptor variants can be accurately diagnosed the prostate cancer [5]. In practical application, different sensors can recognize biomarkers in sweat, tears, saliva, blood and exhalation [6–8], and detect whether the human body has been attacked by corresponding diseases. Peled et al. have described the latest research progress in the application of molecular biomarkers in lung cancer screening, and summarized the discovery of eight possible biomarkers [9]. In liver cirrhosis, Dadamio et al. have determined ketones acetate, 2-butanone and 2-pentanone in the breath of patients with liver disease by gas chromatography-mass spectrometry (GC–MS) [10]. Rio et al. have shown that limonene, CH$_4$O and 2-pentanone are respiratory markers of liver cirrhosis. In other words, whether a person's breath contains limonene, methanol and 2-pentanone can be used to determine whether he is a patient of liver cirrhosis, and it should be emphasized that limonene has the best diagnostic ability in individuals [11].

---

* Corresponding author.
  E-mail address: hecheng@mail.xjtu.edu.cn (C. He).

Optical sensors convert incident light into electrical signals for measurement and analysis. And optical sensors based on traditional detection methods such as absorbance, fluorescence, chemiluminescence and surface plasmon resonance can be used in gas sensing because of their non-invasive, easy to connect, fast response and high sensitivity. Many metal oxides such as WO_3, Fe_3O_4 are often used as sensors, but low visible light absorption and easy aggregation inhibits their application [12,13]. In 2004, researchers have successfully stripped grapheme [14], and thus opened up a new research direction, namely two-dimensional (2D) layered materials [15–17]. With the progress of science and technology, a variety of 2D materials have emerged, including silicene, germanene, stanene, phosphorene and graphene-like carbon nitrogen [18–22]. The application fields of 2D layered materials involve high-speed optoelectronic devices, energy storage, catalysis, chemical sensors and so on [23–28]. In the aspect of sensor, 2D materials not only greatly improve the selectivity and sensitivity of gas sensor, but also reduce the scale, power consumption and working temperature of gas sensor due to its ultra-thin structure, large specific surface area and strong surface activity [29,30]. Therefore, many applications of two-dimensional materials in sensors have been studied, such as adsorption of o-xylene and styrene on 5–8 phosphine sheet, adsorption of pichlorohydrin and phosgene on kagome phosphine molecular devices and so on [31–33]. In order to achieve practical applications, optical sensors need to meet the following criteria: (1) suitable band gap; (2) sufficient active sites; (3) easy synthesis, low cost and large-scale production. Therefore, it is very important to find a low-cost optical sensor with a large number of active adsorption sites. Based on the above criteria, we find that graphite-like carbon-nitride nanosheet have the potential to meet the above three criteria, because of its wide band gap range, low cost, easy access, durability and robustness, non-metallic and environmentally friendly. The previous research has confirmed the feasibility of using C_3N as biosensor to sequence nucleobases [34]. Sun et al. have prepared an adrenaline electrochemical sensor with g-C_3N_4 nanosheet [35]. Zhang et al. have used graphite-like carbon nitride to prepare sensors for measuring ascorbic acid, dopamine and uric acid [36]. Wu et al. have successfully synthesized a novel 2D all carbon isomer graphdiyne by crossing-coupling reaction, and the biosensor prepared by graphdiyne can be used for rapid detection of bisphenol A [37]. Moreover, carbon-nitride materials can be used as sensors in protein, immunoassay, biomolecular detection and other biosensor applications [38–40]. Among them, g-C_6N_6 nanosheet is a semiconductor with the most suitable band gap [41], which is suitable as chemical and biological sensors. And the appropriate band gap means that it has good light response ability. Cao et al. have successfully prepared g-C_6N_6 using the CN stoichiometry method [42]. Since gas molecules undergo charge transfer during adsorption or desorption, changes in band gap are noticed, which can be easily identified as changes in resistance [43]. Moreover, the electronic properties of graphene-like carbon nitride can be controlled by strain and other means [44]. Optical gas sensors have been widely used in safety protection, such as infrared absorption type and spectral absorption type optical gas sensors. Because the absorption peaks of different gases are different, the gas can be detected by analyzing the absorption peaks.

In this work, the atomic structures, electronic properties and adsorption behavior of three liver cirrhosis biomarkers (limonene, CH_4O and 2-pentanone) on g-C_6N_6 monolayer are systematically investigated to illustrate the potential of g-C_6N_6 as a novel liver cirrhosis optical sensor. By calculating the absorption coefficient, the absorption peaks are enhanced after adsorption of limonene, CH_4O and 2-pentanone, indicating that the possibility of g-C_6N_6 monolayer as an optical gas sensor. In addition, the effects of strain and external electric field on the adsorption system are also investigated. After the strain is applied, the adsorption and desorption can be realized effectively. Therefore, g-C_6N_6 monolayer is a potential optical gas sensor for detecting biomarkers of liver cirrhosis.

2. Computational methodology

The first-principles DFT calculations about geometric optimization, total energy, and electronic properties (density of states, density of electrons, and population analysis) were performed within the DMol^3 code. The electron exchange–correlation functional was treated by using the generalized gradient approximation (GGA) with Perdew-Burke-Ernzerhof (PBE) parametrization. The double numerical plus polarization (DNP) basis set and the combined DFT semi-core pseudopotential (DSPP) approximation were used. This replaces the kernel electrons with a single effective potential, and introduces some relativistic correction. Because of the weak long-range interactions between layers, we adopted the Grimme van der Waals correction (DFT-D) to better describe the adsorption of molecules on the surface. We used a $2 \times 2 \times 1$ computational supercell. In order to eliminate the interaction between adjacent periodic sections, the thickness of the vacuum layer was set to 25 Å in the z direction. On behalf of the accuracy of calculation results, the energy threshold, convergence force and self-consistent field (SCF) were set to 1×10^{-5} Ha, 2×10^{-3} Ha / Å and 1×10^{-6} eV respectively, and the maximum displacement is 5×10^{-3} Å. Classical Molecular Dynamics (MD) simulation using NVT ensemble and COMPASS force field further confirmed the dynamic stability of g-C_6N_6 monolayer. In the simulation process, the Andersen method was chosen to control the temperature.

3. Results and discussion

3.1. The geometric stability and electronic properties of g-C₆N₆ monolayer

As shown in Fig. 1(a), the unit cell of g-C_6N_6 is consisted of two C_3N_3 six membered rings connected by C-C bonds, and each C_3N_3 six membered ring is connected by C-N bonds. In order to verify the accuracy of the structure of g-C_6N_6, the atomic structure was firstly optimized. After complete relaxation, the optimized lattice parameters of g-C_6N_6 monolayer are $a = b = 7.13$ Å, and the bond lengths of C-C bond and C-N bond are 1.504 Å and 1.345 Å, respectively. By analyzing the band structure in Fig. 1(b), it is found that g-C_6N_6 monolayer is a semiconductor with direct band gap at K point, and the band gap is 1.631 eV, which is consistent with the previous study[45]. By using HSE06 hybrid functional, We found that the g-C_6N_6 monolayer is still a semiconductor with a direct band gap at K point, and the band gap is enlarged to 3.07 eV(Fig. S1).

The stability of the selected structure can be ensured by the cohesive formation energy. The equation of cohesive formation energy is composed of the energy of g-C_6N_6, the total number of available atoms (x) and the energy of individual atoms [46]. The equation is as follows:

$$E_{coh} = \left(\frac{1}{x}\right)\left[E_{(g-C_6N_6)} - xE_{(C,N)}\right] \tag{1}$$

According to the above equation, the value of cohesive formation energy is calculated as − 6.21 eV/atom. The negative value of E_{coh} further emphasizes the usability of g-C_6N_6 [47]. In Fig. 1(c)-(d), the dynamic stability of g-C_6N_6 is verified by the absence of virtual frequency in phonon spectrum, and the thermal stability of g-C_6N_6 at 300 K is confirmed by MD simulation. Moreover, the exfoliation energy required to peel off an atomic layer from the surface of a bulk material is of fundamental importance in the science and engineering of two-dimensional materials. Therefore, the exfoliation energy per unit area (E_{exf}) was studied and given by the following equation:

$$E_{exf} = \frac{E_{iso} - E_{laters} * \frac{1}{2}}{A} \tag{2}$$

Here, E_{iso} is the unit cell energy of an isolated monolayer in vacuum, E_{layers} is the unit cell energy of a material with two layers, and A is the in-plane area of the bulk unit cell [48]. E_{exf} of g-C_6N_6 is 7.566 meV/Å^2, it can be found that E_{exf} of g-C_6N_6 is smaller than that of graphite (21 meV/

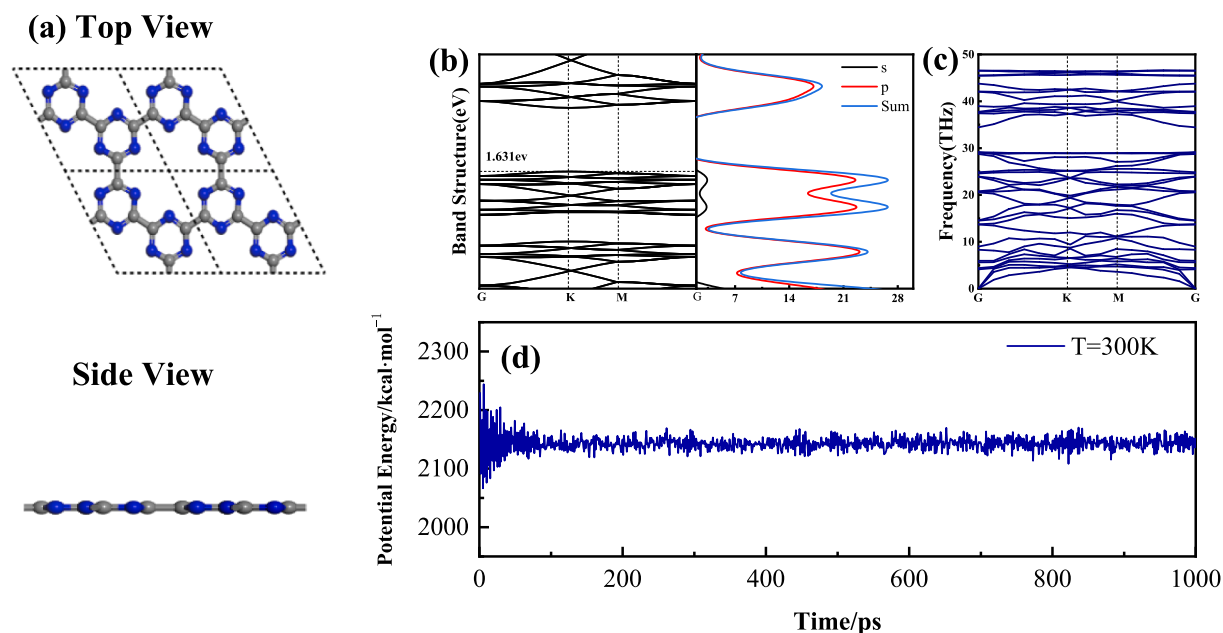**Fig. 1.** Top and side view of g-C_6N_6 monolayer (a), Band gap structure and partial density of states (PDOS) (b), Phonon of g-C_6N_6 monolayer (c), Potential energy curve of g-C_6N_6 in MD simulation (d).

$\mathring{A}^2$), which also indicates that the g-C_6N_6 monolayer can be easily prepared from its bulk forms using a similar experimental mechanical exfoliation method to that of graphene.

3.2. The adsorption studies of g-C_6N_6 monolayer and liver cirrhosis biomarkers

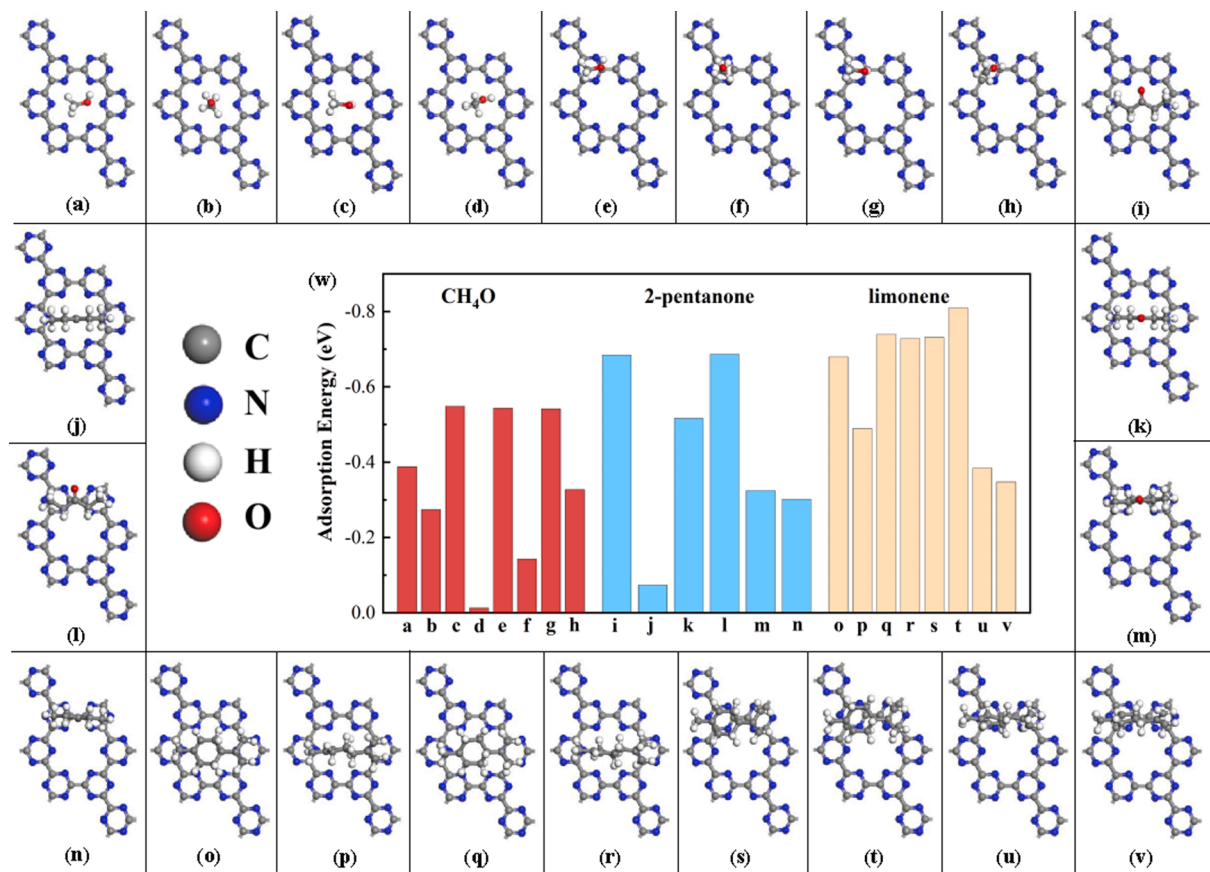When various biomarker gas molecules interact with 2D monolayer,

Fig. 2. A schematic illustration of adsorption of CH_4O (a)-(h), 2-pentanone (i)-(n) and limonene (o)-(v). (w) The adsorption energies of CH_4O, 2-pentanone and limonene on g-C_6N_6 monolayer.

the monolayer will exhibit special responses to these gases. The changes of monolayer before and after adsorption can be understood by electronic energy band diagram, partial density of states, Mulliken charge analysis and electrostatic potential changes. In order to fully understand the interaction between g-C_6N_6 and limonene ($C_{10}H_{16}$), CH_4O (CH_3OH) and 2-pentanone ($C_5H_{10}O$), different adsorption directions and different adsorption positions are considered, as shown in Fig. 2. For liver cirrhosis biomarkers adsorption on g-C_6N_6, there are two available binding sites of adsorption configurations: one is CH_4O (Fig. 2 a-d), 2-pentanone (Fig. 2 i-k) and limonene (Fig. 2 o-r) molecules residing to the center of the large hole, and another is CH_4O (Fig. 2 e-h), 2-pentanone (Fig. 2 l-n) and limonene (Fig. 2 s-v) molecules residing to the six-membered rings. The adsorption energy (E_{ad}) of liver cirrhosis biomarkers on g-C_6N_6 is discussed, which is calculated by the following equation:

$$E_{ad} = E_{(g-C_6N_6/biomarker)} - E_{g-C_6N_6} - E_{biomarker} \qquad (3)$$

where $E_{(g-C_6N_6/biomarker)}$, $E_{g-C_6N_6}$, and $E_{biomarker}$ are the total energies of the fully relaxed system, the isolated substrate, and the isolated gas molecule, respectively. The more negative energy is, the more stable system is, which has been described in previous literature [49]. According to the adsorption energy, the most stable adsorption configurations of the three gases are selected as CH_4O (Fig. 2c), 2-pentanone (Fig. 2i), limonene (Fig. 2t), and the absolute value of adsorption energy for the three gases are 0.55 eV, 0.68 eV and 0.81 eV, respectively. According to the results of the most stable position obtained by adsorption energy, CH_4O and 2-pentanone gas molecules are adsorbed in the center of the large hole of g-C_6N_6 without forming any bond with the monolayer. The best adsorption site of limonene is above two six-membered rings, and there is no bond connection between limonene and monolayer.

In previous research report, when the absolute value of adsorption energy is higher than 0.5 eV, the gas adsorption on the substrate surface can be better realized [50]. The absolute value of adsorption energy for limonene, CH_4O and 2-pentanone on g-C_6N_6 is in the range of 0.55–0.81 eV. These results inspire us to explore the feasibility of g-C_6N_6 as a biomarker gas sensor for liver cirrhosis. The calculated charge transfer (Q) of CH_4O is 0.031e, which indicates that the charge transfer occurs between g-C_6N_6 and CH_4O, and CH_4O acts as a donor. The interaction between ions is weak. Q (0.061e) of 2-pentanone is larger than that of CH_4O, and the adsorption energy (0.68 eV) is also larger. Among them, limonene has a maximum adsorption energy of 0.81 eV. Moreover, compared with CH_4O and 2-pentanone, Q between limonene and substrate (0.077 e) is the largest. The distances between the surface of g-

C_6N_6 monolayer and the adsorbed gas molecules are 2.06 Å, 1.56 Å, 1.49 Å, respectively, which are greater than the sum of the covalent radii of H- C (1.09 Å) and H- N (1.07 Å). The results indicate that limonene, CH_4O and 2-pentanone adsorbed on g-C_6N_6 monolayer are all physical adsorption [51].The number of carbon and hydrogen atoms in the molecular formula of limonene, 2-pentanone and CH_4O are obviously different from the structural formula. It can be considered that in these gases, carbon and hydrogen atoms promote charge transfer, and limonene has the most carbon atoms and hydrogen atoms. So its charge transfer quantity is larger than that of CH_4O and 2-pentanone [52].

The next important parameter to determine the adsorption of biomarkers is the change of energy band and density of states. For g-C_6N_6 monolayer adsorbed with biomarkers, Fig. 3 shows the electronic energy band structures of CH_4O, 2-pentanone, limonene, respectively. It can be noted that when biomarker gas molecules interact with g-C_6N_6 monolayer, the energy band structures are modified, which essentially reflect the influence of gas molecules on monolayer. It can be noted that g-C_6N_6 monolayer adsorbed limonene, CH_4O and 2-pentanone gas molecules are still semiconductors with direct band gaps at K point, but their CBM obviously moves to Fermi level, and the band gaps of limonene, CH_4O and 2-pentanone minimize to 1.148 eV, 1.006 eV and 1.006 eV. The change of band gap of limonene (0.482 eV) is less than that of CH_4O (0.624 eV) and 2-pentanone (0.613 eV). Because there are circulating groups in the molecules, which enlarge the band gaps. The upper and lower parts of the illustrations in Fig. 3 (a), (b) and (c) represent the highest occupied molecular orbital (HOMO) and the lowest unoccupied molecular orbital (LUMO) of g-C_6N_6 monolayer after adsorption of limonene, CH_4O and 2-pentanone. After gas adsorption, the energy level of VBM of g-C_6N_6 monolayer is modified. It can be seen from HOMO and LUMO that gas molecules are easy to lose electrons as electron donors, while g-C_6N_6 monolayer is easy to get electrons as electron acceptor.

As can be seen from Fig. 4(a) and (b), DOS of g-C_6N_6 monolayer adsorbing CH_4O and 2-pentanone have new peaks at −0.01 and −0.02 eV compared with the original g-C_6N_6 monolayer. In Fig. 4(c), there is no new peak in DOS of g-C_6N_6 monolayer after adsorbing limonene. But an obvious fluctuation could be found in the range of −0.63 to 0 eV, which represents the change of electronic properties of g-C_6N_6 monolayer after adsorbing three gases. The electron interaction between the monolayer and the gas also corresponds to the change of the band gap in the energy band diagram. The work function (φ) is also calculated, which is given by the formula:
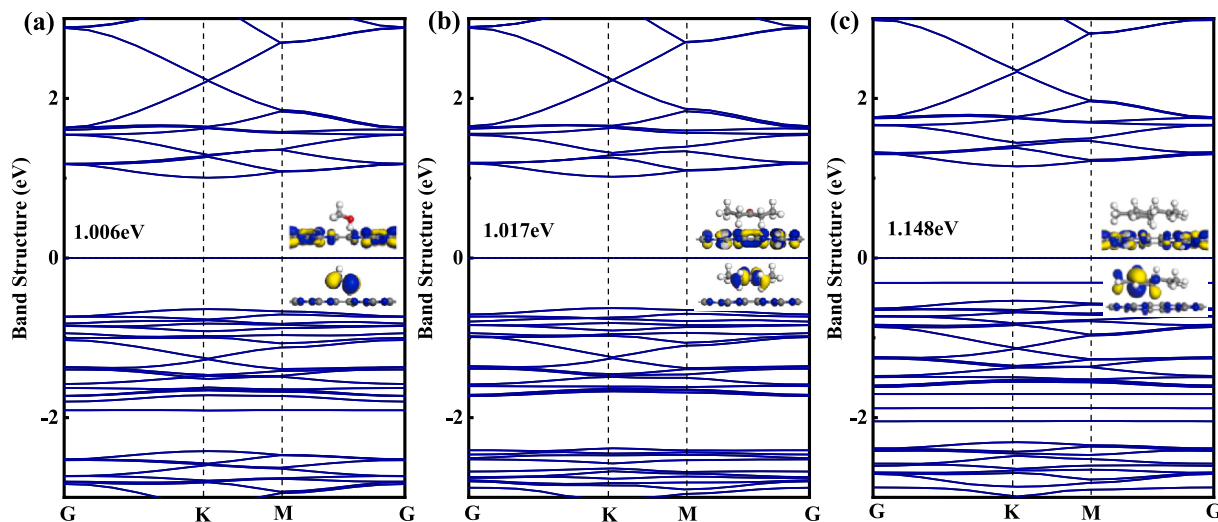
$$\varphi = E_{vac} - E_f \qquad (4)$$

Fig. 3. The energy band structure of g-C_6N_6 monolayer after adsorption of CH_4O (a), 2-pentanone (b) and limonene (c). The Fermi level is set to zero. The upper and lower parts of the illustration represent the highest occupied molecular orbital (HOMO) and the lowest unoccupied molecular orbital (LUMO).
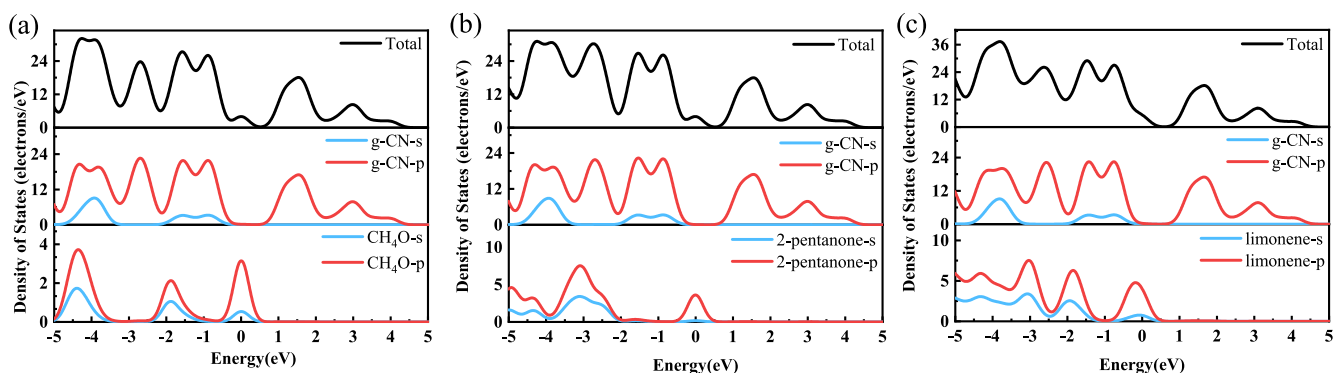
Fig. 4. The partial density of states (PDOS) of g-C_6N_6 monolayer after adsorption of CH_4O (a), 2-pentanone (b) and limonene (c).

where E_{vac} is the electrostatic potential in a vacuum near to the surface. E_f is the electrostatic potential at the Fermi level [53].

Then the charge density difference, electrostatic potential and work function are calculated as shown in Fig. 5. From the diagram of electrostatic potential and charge density difference in Fig. 5 (a)-(d), it can be seen that after adsorption, there is obvious electronic interaction between CH_4O, 2-pentanone and limonene gas molecules and g-C_6N_6 monolayer. As can be seen from Fig. 5 (e), the work functions of CH_4O, 2-pentanone and limonene adsorbed on g-C_6N_6 monolayer are 5.63, 5.61 and 5.66 eV, respectively, which are less than 6.31 eV of the primitive g-C_6N_6 monolayer, indicating that the systems after adsorbing gas have stronger electron affinity than the primitive g-C_6N_6 monolayer. The maximum work function of g-C_6N_6 monolayer adsorbing limonene is 5.66 eV, which is due to the maximum adsorption energy.

3.3. Effects of strain and electric field on adsorption

The adsorption energy should be large enough to indicate that the gas is adsorbed by the substrate. However, considering the recycling use of the sensor, the adsorption energy of the gas should not be too large. Generally speaking, when the absolute value of the adsorption energy is less than 0.5 eV, the gas can be separated by itself to realize recycling use [54]. The absolute values of the adsorption energy of CH_4O, 2-pentanone and limonene are 0.55, 0.68 and 0.81 eV respectively without any regulating. Therefore, it is considered that the adsorption energy could meet the requirements of separation through regulation. In the following, the effects of uniaxial and biaxial strains on g-C_6N_6 monolayer

are investigated, where the negative and positive signs express the compressive and tensile strain, respectively. Because g-C_6N_6 monolayer are anisotropic, uniaxial strain is applied from a and b directions, respectively, and biaxial strain is applied along a-b direction at the same time. The relationship between adsorption energy and strain is shown in Fig. 6. It can be seen that when uniaxial strain is applied from direction a, the adsorption energy continuously becomes positive while uniaxial tensile strain continuously increases. When uniaxial compressive strain is applied, the adsorption energy gradually becomes more negative with increasing compressive stress. When −4% strain is applied, the adsorption energies of CH_4O, 2-pentanone and limonene reach to −1.46, −1.61, −1.75 eV. When uniaxial strain is applied from b direction in Fig. 6 (b), the change trend of adsorption energy is the same as that in a direction. The slope of adsorption energy curve is larger than that of tensile strain, which shows that it is sensitive to compressive strain. Small compressive strain will greatly change the adsorption energy, which is helpful for adsorbing of three biomarkers by g-C_6N_6 monolayer. For biaxial strain, the adsorption energy increases when the compressive strain is applied, and decreases when the tensile strain is applied, which indicates that the structural anisotropy has no significant effect on the applied strain. When + 8% strain is applied, the adsorption energies of CH_4O, 2-pentanone and limonene reach to −0.49, −0.60 and −0.67 eV. And all the adsorption energies of 2-pentanone and limonene changes over 0.1 eV, which is effectively regulated. Generally, electronic properties can be effectively controlled by applying strain and external vertical electric field. In addition, the influence of applying strain and electric field simultaneously on adsorption energy is also considered.
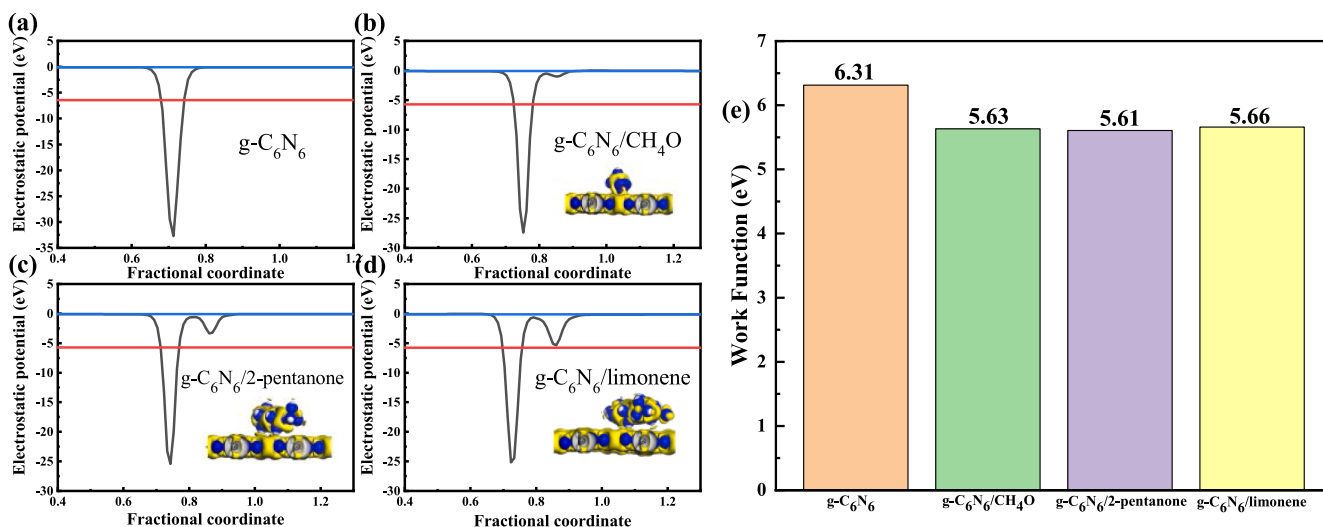

Fig. 5. The electrostatic potential of primitive g-C_6N_6 (a) and after adsorption of CH_4O (b), 2-pentanone (c) and limonene (d), the illustration shows the charge density difference. Work function (e) of g-C_6N_6 upon biomarkers adsorption.
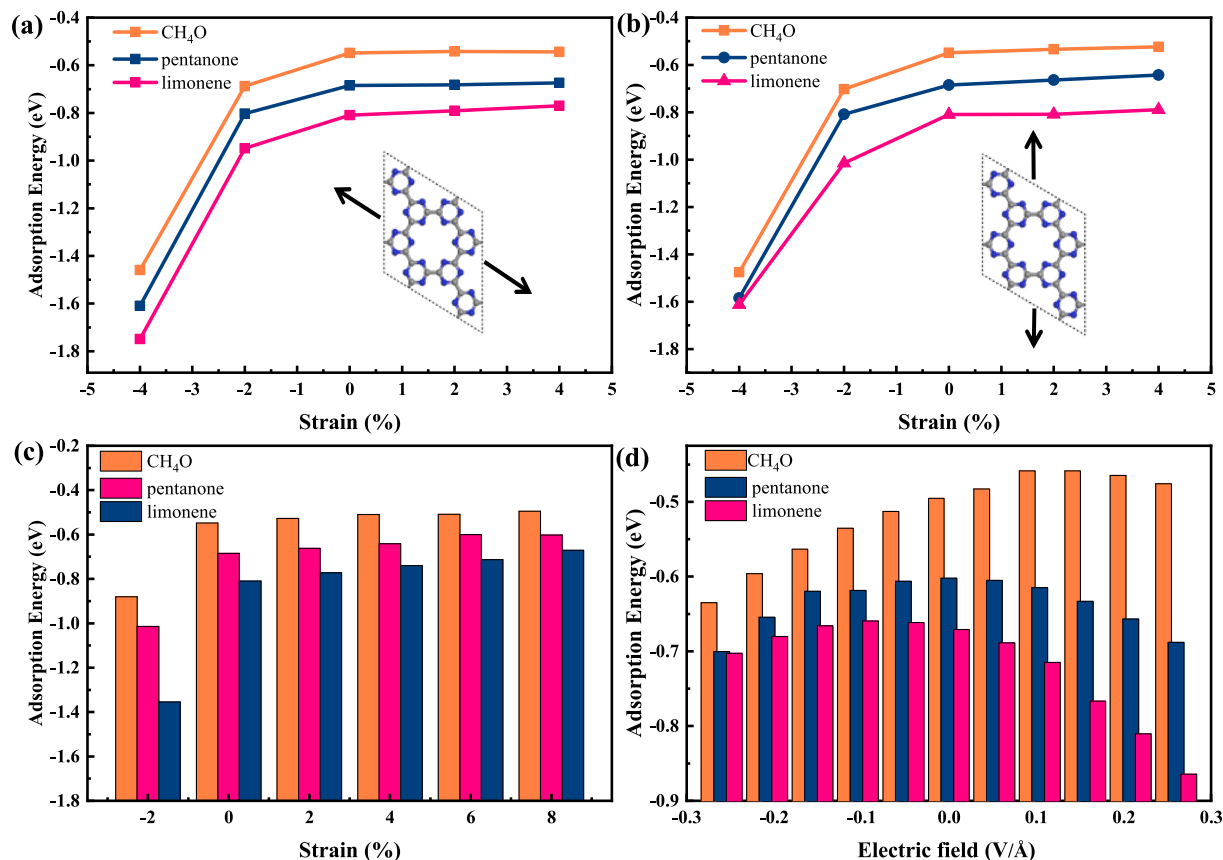
Fig. 6. E_{ads} (in eV) of biomarkers on g-C_6N_6 monolayer with uniaxial strain (a)-(b), biaxial strain (c), and an electric field effect on E_{ads} with $+$ 8% strain (d). The black arrow indicates the direction of the uniaxial strain.

Under the strain of $+$ 8%, an external vertical electric field of -0.26 V/Å to 0.26 V/Å is applied. It can be seen from Fig. 6(d) that in the range of -0.26 V/Å to 0.26 V/Å, all the adsorption energies of g-C_6N_6 monolayer with CH$_4$O, 2-pentanone and limonene become positive at first and then tend to negative.

For CH$_4$O, 2-pentanone and limonene, when an electric field of 0.104 V/Å is applied, the absolute value of the adsorption energy of g-C_6N_6 monolayer to CH$_4$O reaches the minimum and becomes 0.46 eV. When an electric field of 0.052 V/Å is applied, the absolute value of the adsorption energy between g-C_6N_6 monolayer and 2-pentanone reaches the minimum and becomes 0.59 eV. When an electric field of -0.104 V/Å is applied, the absolute value of adsorption energy between g-C_6N_6 monolayer and 2-pentanone reaches the minimum and becomes 0.66 eV. Under the condition of applying electric field, the change of the maximum adsorption energy and the original adsorption energy between g-C_6N_6 monolayer and the three gases is less than 0.02 eV, which indicates that the external vertical electric field has little effect on the adsorption and desorption of the three gases, but the application of electric field can effectively enhance the adsorption of the three gases by g-C_6N_6 monolayer.

3.4. Optical dielectric function of g-C₆N₆ monolayer upon gas adsorption

From the analysis of energy band structure, VBM and CBM are not consistent with g-C_6N_6 before and after gas molecule adsorption, which means that gas adsorption will change the optical properties by the adsorbent materials. In addition, 2D nanomaterials have been proved to be good candidates for optical gas sensors due to their ideal direct semiconductor properties. In order to explore the potential of g-C_6N_6 monolayer as an optical gas sensor, the absorption coefficients with or without strains are calculated. Considering the influence of strain on

optical properties, the strains of $-$ 4% and $+$ 8% are selected for calculation, as shown in Fig. 7. After gas molecules are adsorbed on g-C_6N_6 monolayer, a very unique and attractive scene can be seen through the absorption coefficient of the adsorbed system shown in Fig. 7. The changes are concentrated on the starting position of absorption and the maximum peak, the number of peaks and the heights of these peaks. Before adsorption, g-C_6N_6 has only one main absorption peak at 465 nm, while after adsorption of CH$_4$O, 2-pentanone and limonene, the adsorption starts in the far ultraviolet region. It is worth noting that the interaction between g-C_6N_6 monolayer and gas molecules results in four main absorption peaks, which are enhanced at 63, 179, 230, 437 nm, as shown in the dotted line in Fig. 7 (a). Therefore, it is easy to find that the adsorption in these systems leads to an increase in the maximum peak number of these systems, which implies that the absorption coefficient of molecules adsorbed on g-C_6N_6 monolayer has been practically improved. On the other hand, after the adsorption of CH$_4$O, the main absorption peak is at 431 nm, and the intensity is 865 cm^{-1}. After the adsorption of 2-pentanone, the main absorption peak is at 420 nm, and the intensity is 926 cm^{-1}. After the adsorption of limonene, the maximum absorption peak is at 437 nm, and the intensity is 1051 cm^{-1}. Obviously, the absorption peak increases and the position of the maximum absorption peak changes. The main peak before adsorption is in the blue light region, and the main peak after adsorption is in the purple light region. Under the $+$ 8% strain, the adsorption peaks of different systems show redshift. Especially, the main adsorption peak of limonene is at 497 nm in the blue region. After applying $-$4% strain, the absorption peaks of different adsorption systems appear blue shift, and the position of the main peak moves to the ultraviolet region. But the peak changes to 4823 cm^{-1}, and the intensity is greatly improved. These findings indicate that it is feasible to detect CH$_4$O, 2-pentanone and limonene with optical sensor based on g-C_6N_6 monolayer.
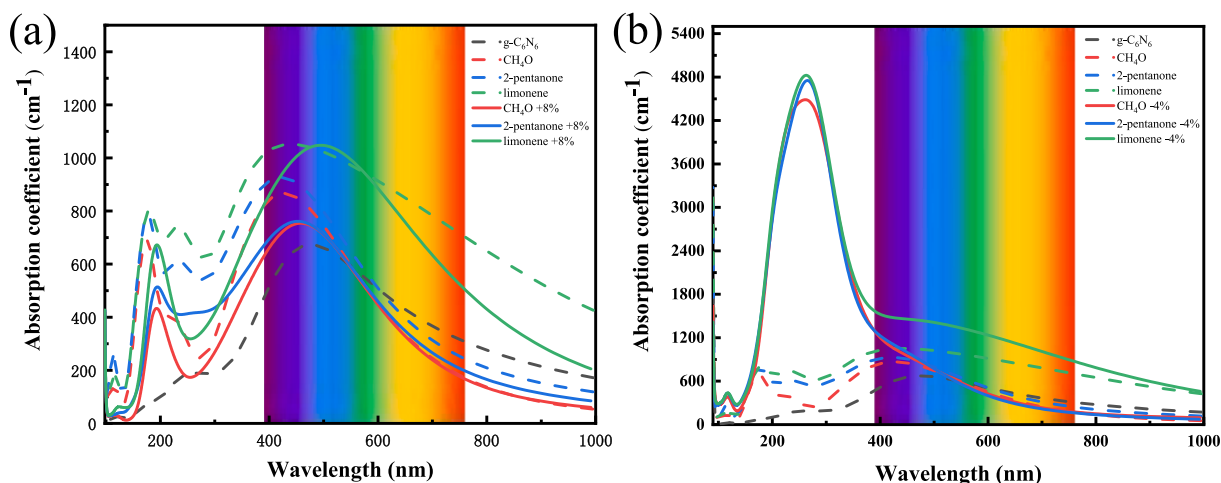
Fig. 7. The absorption coefficient of biomarkers on *g*-C$_6$N$_6$ monolayer with + 8% (a) and −4% (b) biaxial strain, positive value represents tensile strain, negative value represents compressive strain.

4. Conclusion

In this paper, the adsorption behaviors of CH$_4$O, 2-pentanone and limonene on *g*-C$_6$N$_6$ monolayer are investigated by DFT to explore the potential as a gas sensor for liver cirrhosis detection. Our results show that the primitive *g*-C$_6$N$_6$ monolayer is a direct semiconductor with band gap of 1.631 eV. After the adsorption, the band gap obviously changes to 1.006 eV (CH$_4$O), 1.017 eV (2-pentanone) and 1.148 eV (limonene), but they are still direct semiconductors. The adsorption energies of CH$_4$O, 2-pentanone and limonene are 0.55 eV, 0.68 eV and 0.81 eV, respectively, which are physical adsorption. In addition, compression strain can effectively enhance the adsorption of the three biomarker gases. The adsorption energies of CH$_4$O, 2-pentanone and limonene can be enhanced to −1.46, −1.61 and −1.75 eV under the −4% strain, while tensile strain has the potential to meet the gas desorption. In terms of optical properties, *g*-C$_6$N$_6$ monolayer has different responses in visible light region after adsorbing CH$_4$O, 2-pentanone and limonene. When + 8% strain is applied, the absorption peaks of limonene shift to green light region. When −4% strain is applied, the absorption peaks of the three gases move to the ultraviolet direction, and the peak intensity is greatly improved from 1051 cm^{-1} to 4823 cm^{-1}. Hence, *g*-C$_6$N$_6$ monolayer can be used as an optical sensor to detect biomarker gas of liver cirrhosis.

CRediT authorship contribution statement

W.X. Zhang: Conceptualization, Supervision, Investigation, Writing - review & editing. **H.M. Yan Yan:** Investigation, Supervision, Writing - review & editing. **C. He:** Investigation, Supervision, Writing - review & editing.

Declaration of Competing Interest

The authors declare that they have no known competing financial interests or personal relationships that could have appeared to influence the work reported in this paper.

Acknowledgments

Appendix A. Supplementary material

Supplementary data to this article can be found online at https://doi.org/10.1016/j.apsusc.2021.150716.

References

[1] M. Giunta, D. Conte, M. Fraquelli, Role of spleen elastography in patients with chronic liver diseases, World J. Gastroenterol. 22 (2016) 7857–7867.
[2] S.K. Asrani, H. Devarbhavi, J. Eaton, P.S. Kamath, Burden of liver diseases in the world, J. Hepatol. 70 (2019) 151–171.
[3] S.M. Aghaei, A. Aasi, S. Farhangdoust, B. Panchapakesan, Graphene-like BC$_6$N nanosheets are potential candidates for detection of volatile organic compounds (VOCs) in human breath: A DFT study, Appl. Surf. Sci. 536 (2021) 13.
[4] M.D. Davis, B.R. Winters, M.C. Madden, J.D. Pleil, C.N. Sessler, M.A.G. Wallace, C.K. Ward-Caviness, A.J. Montpetit, Exhaled breath condensate biomarkers in critically ill, mechanically ventilated patients, J. Breath Res. 15 (2021), 016011.
[5] H. Saxby, C. Mikropoulos, S. Boussios, An update on the prognostic and predictive serum biomarkers in metastatic prostate cancer, Diagnostics 10 (2020) 549.
[6] C.H. Park, V. Schroeder, B.J. Kim, T.M. Swager, Ionic liquid-carbon nanotube sensor arrays for human breath related volatile organic compounds, ACS Sens. 3 (11) (2018) 2432–2437.
[7] F. Amiripour, S. Ghasemi, S.N. Azizi, A novel non-enzymatic glucose sensor based on gold-nickel bimetallic nanoparticles doped aluminosilicate framework prepared from agro-waste material, Appl. Surf. Sci. 537 (2021) 147827, https://doi.org/10.1016/j.apsusc.2020.147827.
[8] S.K. Arumugasamy, S. Govindaraju, K. Yun, Electrochemical sensor for detecting dopamine using graphene quantum dots incorporated with multiwall carbon nanotubes, Appl. Surf. Sci. 508 (2020) 145294, https://doi.org/10.1016/j.apsusc.2020.145294.
[9] L.M. Seijo, N. Peled, D. Ajona, M. Boeri, J.K. Field, G. Sozzi, R. Pio, J.J. Zulueta, A. Spira, P.P. Massion, P.J. Mazzone, L.M. Montuenga, Biomarkers in lung cancer screening: Achievements, promises, and challenges, J. Thorac. Oncol. 14 (3) (2019) 343–357.
[10] J. Dadamio, S. Van den Velde, W. Laleman, P. Van Hee, W. Coucke, F. Nevens, M. Quirynen, Breath biomarkers of liver cirrhosis, J. Chromatogr. B 905 (2012) 17–22.
[11] R. Fernández del Río, M.E. O'Hara, A. Holt, P. Pemberton, T. Shah, T. Whitehouse, C.A. Mayhew, Volatile biomarkers in breath associated with liver cirrhosis-comparisons of pre- and post-liver transplant breath samples, Ebiomedicine 2 (9) (2015) 1243–1250.
[12] R. Ponnusamy, R. Venkatesan, R. Samal, M. Kandasamy, V. Gandhiraj, B. Chakraborty, C.S. Rout, Bifunctional WO$_3$ microrods decorated RGO composite as catechol sensor and optical limiter, Appl. Surf. Sci. 536 (2021) 147669, https://doi.org/10.1016/j.apsusc.2020.147669.
[13] W. Yang, H. Tian, J. Liao, Y. Wang, L. Liu, L. Zhang, A. Lu, Flexible and strong Fe$_3$O$_4$/cellulose composite film as magnetic and UV sensor, Appl. Surf. Sci. 507 (2020) 145092, https://doi.org/10.1016/j.apsusc.2019.145092.
[14] K.S. Novoselov, A.K. Geim, S.V. Morozov, D. Jiang, Y. Zhang, S.V. Dubonos, I.V. Grigorieva, A.A. Firsov, Electric field effect in atomically thin carbon films, Science 306 (2004) 666–669.
[15] F. Xia, H. Wang, D.i. Xiao, M. Dubey, A. Ramasubramaniam, Two-dimensional material nanophotonics, Nat. Photonics 8 (12) (2014) 899–907.
[16] J.F. Shen, Y.M. He, J.J. Wu, C.T. Gao, K. Keyshar, X. Zhang, Y.C. Yang, M.X. Ye, R. Vajtai, J. Lou, P.M. Ajayan, Liquid phase exfoliation of two-dimensional materials by directly probing and matching surface tension components, Nano Lett. 15 (2015) 5449–5454.

[17] R.R. Liang, S.Y. Jiang, A. Ru-Han, X. Zhao, Two-dimensional covalent organic frameworks with hierarchical porosity, Chem. Soc. Rev. 49 (2020) 3920–3951.

[18] R. Hu, Z. Chen, C. Dai, X. Guo, W. Feng, Z. Liu, H. Lin, Y.u. Chen, R. Wu, Engineering two-dimensional silicene composite nanosheets for dual-sensitized and photonic hyperthermia-augmented cancer radiotherapy, Biomaterials 269 (2021) 120455, https://doi.org/10.1016/j.biomaterials.2020.120455.

[19] B. Mortazavi, O. Rahaman, M. Makaremi, A. Dianat, G. Cuniberti, T. Rabczuk, First-principles investigation of mechanical properties of silicene, germanene and stanene, Physica E 87 (2017) 228–232.

[20] L.K. Cheng, J.H. Meng, X.J. Pan, Y. Lu, X.W. Zhang, M.L. Gao, Z.G. Yin, D.G. Wang, Y. Wang, J.B. You, J.C. Zhang, E.Q. Xie, Two-dimensional hexagonal boron-carbon-nitrogen atomic layers, Nanoscale 11 (2019) 10454–10462.

[21] S. Zhang, Z. Yan, Y. Li, Z. Chen, H. Zeng, Atomically thin arsenene and antimonene: Semimetal-semiconductor and indirect-direct band-gap transitions, Angew. Chem.-Int. Edit. 54 (10) (2015) 3112–3115.

[22] S.L. Zhang, M.Q. Xie, F.Y. Li, Z. Yan, Y.F. Li, E.J. Kan, W. Liu, Z.F. Chen, H.B. Zeng, Semiconducting group 15 monolayers: A broad range of band gaps and high carrier mobilities, Angew. Chem.-Int. Edit. 55 (2016) 1666–1669.

[23] G. Huang, B. Cai, C.F. Zhan, P. Sun, Two-dimensional material as anode for lithium ion batteries: Recent progress, Int. J. Electrochem. Sci. 15 (2020) 5416–5429.

[24] Y.e. Zhou, M. Zhang, Z. Guo, L. Miao, S.-T. Han, Z. Wang, X. Zhang, H. Zhang, Z. Peng, Recent advances in black phosphorus-based photonics, electronics, sensors and energy devices, Mater. Horizons 4 (6) (2017) 997–1019.

[25] Z. Huang, H. Liu, R. Hu, H. Qiao, H. Wang, Y. Liu, X. Qi, H. Zhang, Structures, properties and application of 2D monoelemental materials (Xenes) as graphene analogues under defect engineering, Nano Today 35 (2020) 100906, https://doi.org/10.1016/j.nantod.2020.100906.

[26] W. Yang, Q.H. Lyu, J. Zhao, L.Q. Cao, Y. Hao, H. Zhang, Recent advance in near-infrared/ultrasound-sensitive 2D-nanomaterials for cancer therapeutics, Sci. China-Mater. 63 (2020) 2397–2428.

[27] J. Li, C. Wan, C. Wang, H. Zhang, X. Chen, 2D Material Chemistry: Graphdiyne-based biochemical sensing, Chem. Res. Chin. Univ. 36 (4) (2020) 622–630.

[28] L. Fu, R. Wang, C.X. Zhao, J.R. Huo, C.Z. He, K.H. Kim, W. Zhang, Construction of Cr-embedded graphyne electrocatalyst for highly selective reduction of CO_2 to CH_4: A DFT study, Chem. Eng. J. 414 (2021) 9.

[29] S.S. Varghese, S.H. Varghese, S. Swaminathan, K.K. Singh, V. Mittal, Two-dimensional materials for sensing: Graphene and beyond, Electronics 4 (2015) 651–687.

[30] X.H. Liu, T.T. Ma, N. Pinna, J. Zhang, Two-Dimensional nanostructured materials for gas sensing, Adv. Funct. Mater. 27 (2017) 30.

[31] R. Bhuvaneswari, V. Nagarajan, R. Chandiramouli, Red tricycle phosphorene nanoribbon as a removing medium of sulfadiazine and sulfamethoxazole molecules based on first-principles studies, J. Mol. Liq. 336 (2021), 116294.

[32] R. Bhuvaneswari, V. Nagarajan, R. Chandiramouli, First-principles research on adsorption properties of o-xylene and styrene on 5–8 phosphorene sheets, Chem. Phys. Lett. 765 (2021) 10.

[33] J.P. Maria, R. Bhuvaneswari, V. Nagarajan, R. Chandiramouli, Kagome phosphorene molecular device for sensing chloropicrin and phosgene ? A first-principles study, Chem. Phys. Lett. 771 (2021) 11.

[34] S. Rani, S.J. Ray, Two-dimensional C_3N based sub-10 nanometer biosensor, Phys. Chem. Chem. Phys. 22 (2020) 11452–11459.

[35] Y.A. Sun, Y. Wang, Y.W. Yang, M.L. Yang, An electrochemiluminescent sensor for epinephrine detection based on graphitic carbon nitride nanosheet/multi-walled carbon nanotubes nanohybrids, Chem. Lett. 48 (2019) 215–218.

[36] L.H. Zhang, C.D. Liu, Q.W. Wang, X.H. Wang, S.T. Wang, Electrochemical sensor based on an electrode modified with porous graphitic carbon nitride nanosheets (C_3N_4) embedded in graphene oxide for simultaneous determination of ascorbic acid, dopamine and uric acid, Microchim. Acta 187 (2020) 10.

[37] L.X. Wu, J. Gao, X.B. Lu, C.S. Huang, Dhanjai, J.P. Chen, Graphdiyne: A new promising member of 2D all-carbon nanomaterial as robust electrochemical enzyme biosensor platform, Carbon, 156 (2020) 568–575.

[38] N. Rohaizad, C.C. Mayorga-Martinez, M. Fojtu, N.M. Latiff, M. Pumera, Two-dimensional materials in biomedical, biosensing and sensing applications, Chem. Soc. Rev. 50 (2021) 619–657.

[39] H. Gu, H.L. Tang, P. Xiong, Z.H. Zhou, Biomarkers-based biosensing and bioimaging with graphene for cancer diagnosis, Nanomaterials 9 (2019) 24.

[40] C.Z. Zhu, D. Dan, Y.H. Lin, Graphene and graphene-like 2D materials for optical biosensing and bioimaging: a review, 2D Mater., 2 (2015) 17.

[41] Y. Zhi, G.Z. Wang, M.L. Bo, J.J. He, M.M. Zhong, W.X. Zhao, Y.D. Li, X.J. Long, W. L. Zhang, Enhanced photocatalytic performance of CdO/g-C_6N_6 heterostructure, Mater. Res. Express 6 (2019) 6.

[42] C.B. Cao, F.L. Huang, C.T. Cao, J. Li, H. Zhu, Synthesis of carbon nitride nanotubes via a catalytic-assembly solvothermal route, Chem. Mat. 16 (2004) 5213–5215.

[43] H.J. Kim, J.H. Lee, Highly sensitive and selective gas sensors using p-type oxide semiconductors: Overview, Sens. Actuator B-Chem. 192 (2014) 607–627.

[44] Y.Z. Abdullahi, T.L. Yoon, M.M. Halim, M.R. Hashim, T.L. Lim, Mechanical and electronic properties of graphitic carbon nitride sheet: First-principles calculations, Solid State Commun. 248 (2016) 144–150.

[45] Y.Z. Abdullahi, T.L. Yoon, A.A. Kassimu, Metal-free ferromagnetic semiconductor: Mechanical, electronic and magnetic properties of boron doped graphitic carbon nitride (g-C_6N_6) sheet, Mater. Chem. Phys. 254 (2020), 123470.

[46] S. Khan, M. Yar, N. Kosar, K. Ayub, M. Arshad, M.N. Zahid, T. Mahmood, First-principles study for exploring the adsorption behavior of G-series nerve agents on graphdyine surface, Comput. Theor. Chem. 1191 (2020) 11.

[47] R. Bhuvaneswari, V. Nagarajan, R. Chandiramouli, Chemisorption of heptachlor and mirex molecules on beta arsenene nanotubes: A first-principles analysis, Appl. Surf. Sci. 537 (2021) 12.

[48] T.T. Li, C. He, W.X. Zhang, Two-dimensional porous transition metal organic framework materials with strongly anchoring ability as lithium-sulfur cathode, Energy Storage Mater. 25 (2020) 866–875.

[49] L. Liu, L. Wu, B. Liu, J. Hou, C. Fang, A. Du, Y. Tang, H. Zhang, Strain induced variation of PFOS adsorption on pristine and defected phosphorene: A DFT study, Appl. Surf. Sci. 532 (2020) 147452, https://doi.org/10.1016/j.apsusc.2020.147452.

[50] H.Y. Guo, W.H. Zhang, N. Lu, Z.W. Zhuo, X.C. Zeng, X.J. Wu, J.L. Yang, CO_2 capture on h-BN sheet with high selectivity controlled by external electric field, J. Phys. Chem. C 119 (2015) 6912–6917.

[51] S.S.A. Al-Abbas, M.K. Muhsin, H.R. Jappor, Two-dimensional GaTe monolayer as a potential gas sensor for SO_2 and NO_2 with discriminate optical properties, Superlattices Microstruct. 135 (2019) 11.

[52] U. Srimathi, V. Nagarajan, R. Chandiramouli, Germanane nanosheet as a novel biosensor for liver cirrhosis based on adsorption of biomarker volatiles - A DFT study, Appl. Surf. Sci. 475 (2019) 990–998.

[53] C. He, F.S. Han, J.H. Zhang, W.X. Zhang, The In$_2$SeS/g-C$_3$N$_4$ heterostructure: a new two-dimensional material for photocatalytic water splitting, J. Mater. Chem. C 8 (2020) 6923–6930.

[54] J.H. Liu, L.M. Yang, E. Ganz, Electrocatalytic reduction of CO_2 by two-dimensional transition metal porphyrin sheets, J. Mater. Chem. A 7 (2019) 11944–11952.